Image Restoration via Nonstandard Diffusion

Stacey Levine and Jon Stanich

Duquesne University
440 College Hall
Department of Math and Computer Science
Pittsburgh, PA 15282

Yunmei Chen

University of Florida
P.O. Box 118105
Department of Mathematics
Gainesville, Florida 32611

Abstract

We present a functional of nonstandard growth for which the corresponding minimization problem provides a model for image denoising, enhancement, and restoration. The diffusion resulting from the proposed model is a combination of isotropic and anisotropic diffusion. Isotropic diffusion is used at locations with low gradient and total variation based diffusion is used along likely edges. At all other locations, the type of anisotropy varies according to the local image information. Experimental results illustrate the effectiveness of the model in removing noise and retaining sharp edges while avoiding the 'staircasing effect'. Existence and uniqueness of the proposed model are also established.

1. Introduction

Over the past 20 years, the use of variational methods and nonlinear partial differential equations (PDEs) has significantly grown and evolved to address the image restoration problem. Here we consider image restoration as the classical inverse problem in which a piecewise smooth image is recovered from noisy data. The challenging aspect of this problem is to design methods which can selectively filter extraneous information, such as noise, without losing significant features or creating false ones. Many nonlinear models have been proposed for this purpose, however, when an image consists of objects of nonuniform intensity or has been degraded by noise, some of the most successful noise removal techniques which retain and even enhance sharp edges often exhibit a 'staircasing effect'. This can result in the generation of false edges which may in turn yield an incorrect segmentation. Our goal is to study a new model for image restoration which not only removes noise and retains sharp edges, but also avoids staircasing in what should be smooth regions.

Current PDE-based image restoration models can be classified into three types: curvature driven diffusion, tensor driven diffusion, and variational methods. Curvature based models diffuse only along the level curves of an image u (in particular, not at all in the direction ∇u), so edges are preserved in the denoising process. The speed of the diffusion depends on the local curvature, and is often penalized where the magnitude of the image gradient is large [2, 8, 13, 15, 16, 18, 19, 20, 25]. Tensor driven diffusion is governed by a matrix built into the diffusion equation [10, 12, 28, 29]. The diffusion governed by this type of model is anisotropic and the matrix determines the direction(s) of the diffusion as well as the speed in each direction. The main feature of this model is that the eigenvalues of the matrix can be chosen so the model can enhance specific features such as edges or textures.

A large number of image restoration techniques are conveniently formulated using a variational approach. The Mumford-Shah functional [17] is often used as a prototype for the free discontinuity problem. When used for image restoration and segmentation, the main characteristic of the Mumford-Shah model is that it diffuses isotropically while minimizing the lengths of the edges. The classic Rudin-Osher-Fatemi model [22] which minimizes the total variation of an image yields diffusion strictly along the level curves of an image. Models based on this method are very successful at recovering piecewise constant images with sharp edges since diffusion is only in the direction orthogonal to ∇u [21, 22, 24, 25, 26, 27].

For images where objects are represented by non-uniform intensities, edges cannot be defined as the boundaries of homogeneous regions. Furthermore, in highly degraded images, diffusion which is strictly in one direction may

create false edges, the phenomenon often referred to as 'staircasing' (see figures 2 and 3). In these cases, one may want more flexibility in both the direction and speed of the diffusion. One solution is to diffuse isotropically away from edges and anisotropically near likely edges. This feature does not occur in any of the three above mentioned classes of models and although it has been explored in the literature, [9, 3, 23, 4, 5, 7], often either the interpolation between isotropic and anisotropic diffusion is difficult to control, or the mathematical foundations are difficult to establish.

In this paper we propose a new image reconstruction model which preserves fine structures and object boundaries with low gradient while avoiding the 'staircasing effect' in piecewise smooth images. This is done using anisotropic diffusion which is between isotropic and total variation (TV) based. The type of anisotropy depends on the local image information, thus providing a natural control of the interpolation. We use a variational approach, as it allows us to express the model using a concise formulation which can be studied mathematically and implemented using straightforward finite difference methods.

The paper is organized as follows. In section 2 we discuss models which combine isotropic and TV-based diffusion and introduce the proposed model. Our numerical schemes are presented in section 3 and experimental results in section 4. Section 5 is our concluding remarks.

2. Combining isotropic and TV-based diffusion

2.1 Background

Several models combining isotropic and TV-based diffusion have been proposed in the literature. Chambolle and Lions [9] proposed the minimization problem

$$\min_{u\in H^1(\Omega)} \frac{1}{2\epsilon}\int_{|\nabla u|<\epsilon} |\nabla u|^2 + \int_{|\nabla u|\geq\epsilon} |\nabla u| - \frac{\epsilon}{2}. \tag{1}$$

This model diffuses strictly perpendicular to the gradient where $|\nabla u| \geq \epsilon$ (where edges are most likely present) and isotropically in regions where $|\nabla u| < \epsilon$. In images where homogeneous regions are separated by distinct edges, (1) yields good restoration results. However, this model can be very sensitive to the threshold ϵ as seen in figures 1, 4 and 5.

Blomgren, Chan, Mulet, and Wong [4, 6] proposed the minimization problem

$$\min \int_\Omega |\nabla u|^{p(|\nabla u|)} dx \tag{2}$$

where

$$\begin{gathered} \lim_{s\to 0} p(s) = 2 \\ \lim_{s\to\infty} p(s) = 1 \\ p(s) \text{ is monotone decreasing} \end{gathered} \tag{3}$$

and $\Omega \subset R^2$ is the image domain. Experimental results in [4] show this model is promising for restoring piecewise smooth images. However it is not readily evident that (2) is lower semi-continuous, making its mathematical analysis very difficult. Furthermore, continually updating the exponent may cause oversmoothing (see figure 1) as well as add to the computation time.

2.2 The Proposed Model

In this paper, we propose the following model which minimizes the nonstandard growth functional

$$\min_{u\in BV(\Omega)\cap L^2(\Omega)} \int_\Omega \phi(x,\nabla u) + \frac{\lambda}{2}|u-I|^2 \tag{4}$$

where I is the observed noisy image, and

$$\phi(x,r) := \begin{cases} \frac{1}{p(x)}|r|^{p(x)}, & |r|<\epsilon \\ |r| - \frac{p(x)-1}{p(x)}, & |r|\geq\epsilon \end{cases}, \tag{5}$$

where $\epsilon > 0$ is fixed, $p(x) = p(|\nabla \widetilde{I}(x)|)$ satisfies (3), $x \in \Omega$ where $\Omega \subset R^2$ is the image domain, and $\widetilde{I}$ is a smoothed version of I. The last term in (4) is a fidelity term.

The main characteristic of (4-5) is that at each different location in the image, the speed and the direction of the diffusion depends on the local image information. At locations with sufficiently large gradient, most likely edges, only TV-based diffusion is used. Where the gradient is close to zero, most likely homogeneous regions, the diffusion is isotropic. At all other locations, $1 < p < 2$ so the diffusion is between isotropic and TV-based. More specifically, at these ambiguous regions the type of anisotropy varies depending on the strength of the gradient. Therefore, in addition to switching between isotropic and anisotropic diffusion, the type of anisotropy will change depending on the local properties of the image. This solves the problem arising from (1) where the denoising can be too sensitive to the choice of threshold. Furthermore, this also enables the model to avoid staircasing in what should be smooth regions.

Not only is (4-5) an effective image reconstruction model, but it is also mathematically sound. In particular, the minimization problem (4-5) admits a unique solution (see appendix) in $BV(\Omega) \cap L^2(\Omega)$, the set of square integrable functions of bounded variation. Furthermore, in [11] we prove that if the initial image $I \in BV(\Omega)$, then there exists a unique solution, $u(x,t) \in BV(\Omega \times R^+)$ of flow associated with (4)-(5) which converges to the solution of (4) as $t \to \infty$.

Before further analysis of (4-5), we give a simple illustration of the effectiveness of the model. In figure 1 we compare the proposed model with TV-based diffusion, diffusion which switches between isotropic and TV-based (1), and diffusion in which the exponent is recomputed at each iteration (2-3). Our goal was to reconstruct an artificial image that had been degraded by additive Gaussian noise with mean 0 (SNR=1:6). When using models (1), (2-3), and (4-5), we illustrated the behavior of the diffusion using 'direction maps' which display blue in regions using only TV-based diffusion ($p \equiv 1$), white in regions using pure isotropic diffusion ($p \equiv 2$), and green where the diffusion is a combination of both isotropic and TV-based ($1 < p < 2$). In the first row of figure 1, we see the noisy image and the reconstruction and edge map using TV-based denoising only. Edges are sharply preserved, but the reconstructed image exhibits the staircasing effect thus creating false edges. In the second and third rows, we tested (1) with the threshold $\epsilon = 30$ and 150 respectively. As the threshold grows, the model recovers smoother regions, but finds it increasingly difficult to reconstruct sharp edges. In the fourth and fifth rows we tested the proposed model (4-5) for the same thresholds, $\epsilon = 30$ and 150. Notice that sharp edges and corners are preserved with both, but there is little to no evidence of staircasing. Furthermore, the model does not show much sensitivity to the threshold, ϵ. In the last two rows, we tested (2) for the same thresholds, $\epsilon = 30$ and 150 and saw similar results, however, there is some evidence of oversmoothing when the threshold becomes large. In this case the main advantages of (4-5) are computation speed (see table 1), less sensitivity to the threshold, and it's mathematical validity.

3. Numerical Methods

Since the desired behavior (in particular, the different types of diffusion) is encoded directly into the model (4-5), the implementation can be done using straightforward finite difference methods.

To this end, we solve the minimization problem (4) numerically using finite differences which approximate the flow of the Euler-Lagrange equation associated with (4), specifically

$$\frac{\partial u}{\partial t} - \operatorname{div}\left(\phi_r(x, Du)\right) + \lambda(u - I) = 0, \qquad \text{in } \Omega \times [0,T] \tag{6}$$

$$\frac{\partial u}{\partial n}(x,t) = 0, \qquad \text{on } \partial\Omega \times [0,T] \tag{7}$$

$$u(0) = I, \qquad \text{in } \Omega \tag{8}$$

For our simulations, we chose $p(x) = p(|\nabla I_\sigma(x)|)$ satisfying (3) to be

$$p(x) = 1 + \frac{1}{1 + k|\nabla G_\sigma * I(x)|^2} \tag{9}$$

where $k, \sigma > 0$ and $G_\sigma(x) = \frac{1}{\sigma} exp\left(-|x|^2/4\sigma^2\right)$ is the Gaussian filter.

There are two main issues to consider:

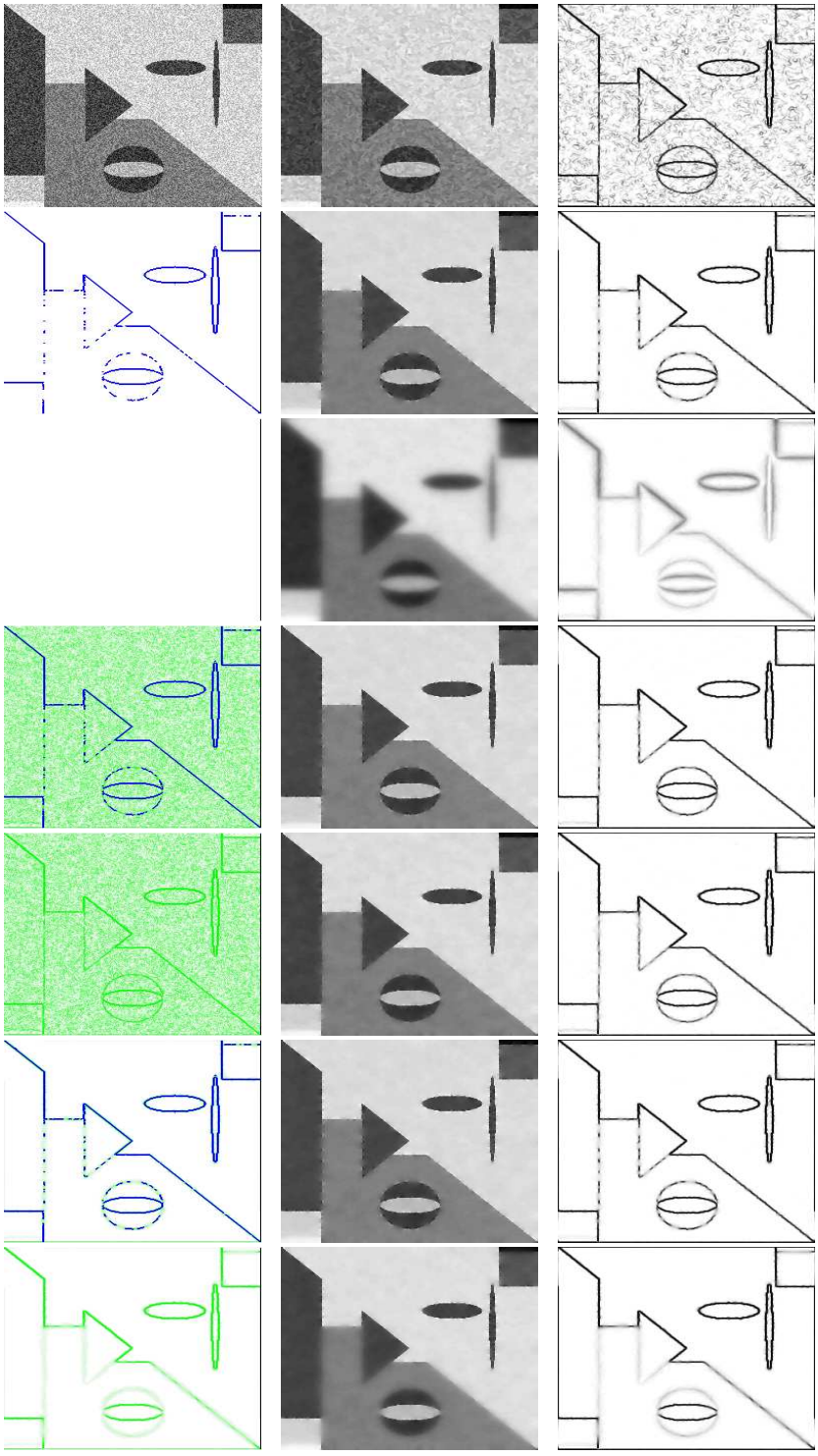

Figure 1: **First Row**: noisy image, reconstruction and edge map using TV restoration only ((1) with threshold $\epsilon = 0$), iterations = 1000; **Second Row**: direction map, reconstruction and edge map for (1) with $\epsilon = 30$, iterations = 500; **Third Row**: direction map, reconstruction and edge map for (1) with $\epsilon = 150$, iterations = 500; **Fourth Row**: direction map, reconstruction and edge map for (4-5) with $\epsilon = 30$, iterations = 500; **Fifth Row**: 5^{th} Row: direction map, reconstruction and edge map for (4-5) with $\epsilon = 150$, iterations = 500; **Sixth Row**: direction map, reconstruction and edge map for (2-3) with $\epsilon = 30$, iterations = 500; **Seventh Row**: 5^{th} Row: direction map, reconstruction and edge map for (2-3) with $\epsilon = 150$, iterations = 500; (all images: $c, k = .0025$, spatial resolution = 256×256)

1. Since the local image information determines the value of p we assume that p is constant when computing the flow of the Euler-Lagrange equation associated with (4). This is reasonable since the model is based on the value of p at a given location and not on the variation of p there.

2. The diffusion is degenerate. Therefore, motivated be the approximation scheme presented in [1], we approximate $\phi(x,r)$ by

$$\phi_\beta(x,r) := \begin{cases} \frac{1}{p(x)}\sqrt{|r|^2+\beta^2}^{p(x)}, & |r|<\epsilon \\ \sqrt{|r|^2+\beta^2}-\frac{p(x)-1}{p(x)}, & |r|\geq\epsilon \end{cases}, \tag{10}$$

for a small parameter $\beta > 0$.

Our difference scheme is as follows. Let h represent the spatial step size and Δt the time step size. Denote $u_{ij} = u(x_i, y_j)$ and $u^n_{ij} = u(x_i, y_j, t_n)$ where $x_i = ih$, $y_j = jh$ and $t_n = n\Delta t$. Since the diffusion term is approximated using central differences, we use the following notation for simplicity:

$$\Delta_x = \frac{u^n_{i+1,j} - u^n_{i-1,j}}{2h},\ \Delta_y = \frac{u^n_{i,j+1} - u^n_{i,j-1}}{2h}$$

$$\Delta_{xx} = \frac{u^n_{i+1,j} - 2u^n_{ij} + u^n_{i-1,j}}{h^2}$$

$$\Delta_{yy} = \frac{u^n_{i,j+1} - 2u^n_{ij} + u^n_{i,j-1}}{h^2}$$

$$\text{and}\ \ \Delta_{xy} = \frac{u^n_{i+1,j+1} - u^n_{i+1,j-1} - u^n_{i-1,j+1} + u^n_{i,j-1}}{h^2}.$$

Then taking

$$\operatorname{div}\left((\phi_\beta)_r(x,Du)\right)^n_{ij} = \begin{cases} \frac{(\Delta_x^2+\Delta_y^2+\beta^2)(\Delta_{xx}+\Delta_{yy})+(p-2)(\Delta_x^2\Delta_{xx}+2\Delta_x\Delta_y\Delta_{xy}+\Delta_y^2\Delta_{yy})}{(\Delta_x^2+\Delta_y^2+\beta^2)^{\frac{4-p}{2}}}, & \sqrt{\Delta_x^2+\Delta_y^2}<\epsilon \\ \frac{\beta^2(\Delta_{xx}+\Delta_{yy})+\Delta_{xx}\Delta_y^2-2\Delta_x\Delta_y\Delta_{xy}+\Delta_{yy}\Delta_x^2}{(\Delta_x^2+\Delta_y^2+\beta^2)^{\frac{3}{2}}}, & \sqrt{\Delta_x^2+\Delta_y^2}\geq\epsilon \end{cases},$$

our scheme is simply

$$u^{n+1}_{ij} = u^n_{ij} + \Delta t\left(\operatorname{div}\left((\phi_\beta)_r(x,Du)\right)^n_{ij} + \lambda(u^n_{ij} - I^n_{ij})\right).$$

4 Experimental Results

In the following, we have compared the results of (4-5) with comparable, mathematically valid methods, in particular, TV-based denoising and (1). We have included the reconstructions, their edge maps, and, when the *type* of diffusion varies depending on the location of the image, the direction maps. The edge maps were constructed using $\frac{1}{1+c|\nabla G_\sigma * u|^2}$ where $c > 0$ is a constant and $G_\sigma(x) = \frac{1}{\sigma}exp\left(-|x|^2/4\sigma^2\right)$ is the Gaussian filter with scale σ. Since all of our images consistently ranged from 0 to 255 we found that a value of $0.025 < c < 0.0025$ and $\sigma = 0.5$ gave the best edge map across all three models. The optimal value of c varied slightly between images, but not between models. Furthermore, optimal results were consistently found for the proposed model (4-5) by choosing the parameter $k > 0$ in the diffusion exponent, $p(x) = 1 + \frac{1}{1+k|\nabla G_\sigma * u|^2}$ within the same range, $0.025 \leq k \leq 0.0025$. As mentioned in section 2, the direction map displays the *type* of diffusion, specifically, it displays white at locations where the diffusion is isotropic, $p(x) \equiv 2$, blue in locations where the diffusion is strictly orthogonal to the gradient, $p(x) \equiv 1$, and green when the diffusion is somewhere in between, $1 \leq p(x) \leq 2$. In all of the examples, our stopping criteria was met when the standard deviation between two consecutive iterations was less than 10^{-3}. Finally, to ensure stability as well as optimal results we choose $\beta = 1$, and our step sizes to be $h = 1$, $\Delta t = 0.05$.

We also compared the CPU time per iteration of each of the models we tested. Model (1) was the fastest, likely due to the fact that simple, linear diffusion is used at most locations. The proposed model (4-5) is not much slower than TV-based denoising alone. The following chart gives an idea of the computation time involved using code written in java and run on a laptop running Windows XP (Mobile Intel(R) Pentium(R) 4-M CPU 2.40GHz; 512 MB of RAM). The models are listed in order of speed.

Table 1: CPU times of TV, (1), (2-3), and (4-5).

Model	spatial res: 100×100 200 iterations	spatial res: 256×256 200 iterations
(1)	1.4 s	11 s
TV only	3 s	22 s
(4-5)	4 s	27 s
(2)	6 s	45 s

Figure 2 illustrates the proposed model's ability to reconstruct piecewise smooth regions while avoiding the staircasing effect. The first row contains a piecewise smooth image, it's edge map, and then the image degraded by Gaussian noise with mean zero. The second row contains reconstructions using isotropic diffusion only ($p \equiv 2$), TV-based diffusion only ($p \equiv 1$), and then the proposed model. In the next row we see their corresponding edge maps. Isotropic diffusion reconstructs smooth regions, but edges are severely blurred. TV-based diffusion reconstructs sharp edges, but the 'staircasing effect' is clearly present. This in turn creates false edges which could lead to an incorrect segmentation of the image. The proposed model reconstructs sharp edges as effectively as TV-based diffusion *and* recovers smooth regions as effectively as pure isotropic diffusion (in particular, without staircasing). The surface views in figure 3 give another perspective of these reconstructed images which illustrates the above mentioned behavior.

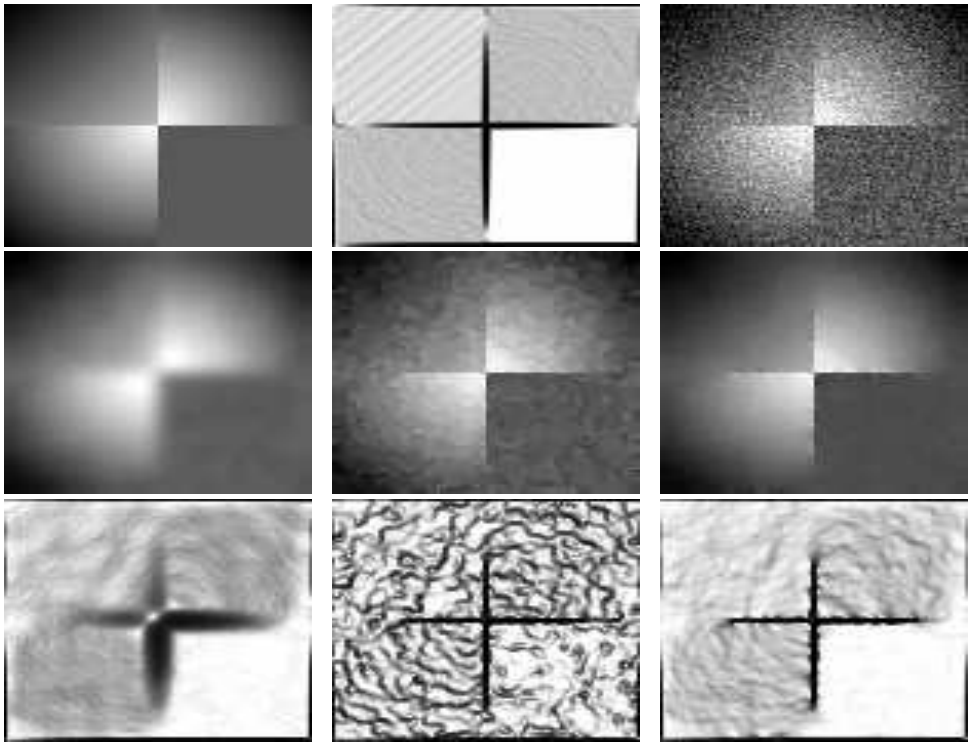

Figure 2: **Top Row**: true image, edge map of the true image, image + noise; **Middle Row**: reconstructed image using isotropic diffusion only (iterations = 100), reconstructed image using TV-based diffusion only (iterations = 3000), reconstructed image using the proposed model (threshold $\epsilon = 30$, iterations = 1500; **Bottom Row**: corresponding edge maps (all images: $c, k = 0.025$, spatial resolution = 100×100)

Figure 4 shows the reconstruction of a radar image of land mines. The goal is to detect the boundaries of the mines without picking up background noise. We compare reconstructions using the proposed model with those using TV-based diffusion only and (1). The first column has the original image, the reconstruction using TV-based diffusion only, and the edge map after applying TV-regularization. Notice that the land mines are sharply traced, but false edges are created in what should be smooth regions. For the other simulations, we include the direction

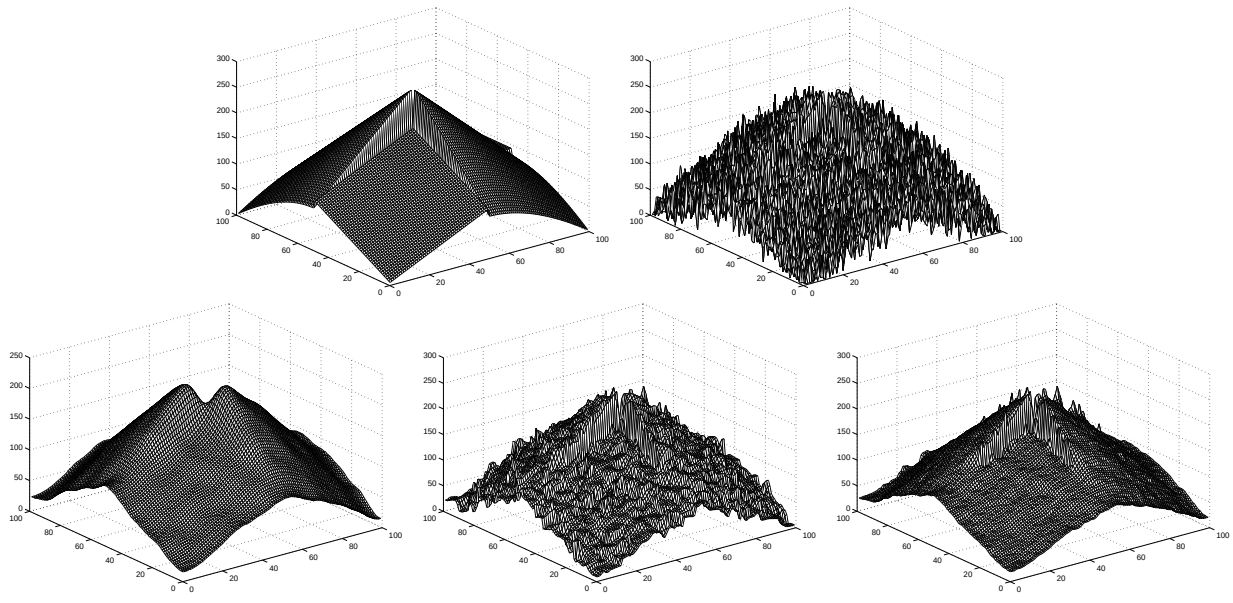

Figure 3: Another view of images in figure 2. **Top Row**: true image, image + noise; **Middle Row**: reconstructed image using isotropic diffusion only (iterations = 100), reconstructed image using TV-based diffusion only (iterations = 3000), reconstructed image using proposed model (threshold $\epsilon = 30$, iterations = 1500, $k = 0.025$)

map which illustrates the type of diffusion at each location in the image (blue represents $p \equiv 1$, white $p \equiv 2$, and green $1 < p < 2$). In the second column we reconstructed the image using (1) with $\epsilon = 25$. There is less background noise, but the boundaries of the mines are no longer as sharp. In the third and fourth columns we used (4-5) with threshold $\epsilon = 25$ and 100 respectively. The boundaries of the mines are just as sharp as as TV-based reconstruction, but the background noise is reduced, helping to avoid the problem of detecting false edges. Furthermore, although the type of diffusion at the edges has changed (which is evident in the direction maps), the model does not display much sensitivity to the threshold.

In figure 5, we reconstruct the 'Lena' image which has been degraded with additive Gaussian noise. This gives another example where the proposed model is able to reconstruct sharp edges and nonuniform regions while avoiding staircasing. In the first row we have the original and degraded images, and can see that TV-based diffusion alone creates false edges. The second and third rows contain the reconstructions using (1) and (4-5) respectively. Again, the proposed model (4-5) reconstructs smooth regions and sharp edges while avoiding staircasing. On the other hand, (1) reconstructs smooth regions, but begins to blur edges as well as lose features with low contrast (e.g. the mouth).

In figures 6 and 7 we used the proposed model to reconstruct two different MRI images, the former with additive Gaussian noise and the latter with noise acquired through the instrument. In both cases, the proposed model removes noise and retains sharp object boundaries without displaying a false segmentation which could result from staircasing. Figure 8 contains an ASTER (Advanced Spaceborne Thermal Spaceborne Emission and Reflectance Radiometer) image of part of the Phoenix, Arizona valley; the region in the bottom right hand corner has been burned by a wildfire. The proposed model does well delineating the boundary between the burned and unburned regions without creating any false edges from the background textures.

5 Conclusion

In this paper we have proposed a new model for image restoration. The model uses both isotropic and anisotropic diffusion for noise removal. The novel aspect of this model is that the type of anisotropy is determined at each individual location in the image, depending on the local image information. This enables the model to remove noise and retain sharp edges without exhibiting staircasing. Our experimental results show that this model is

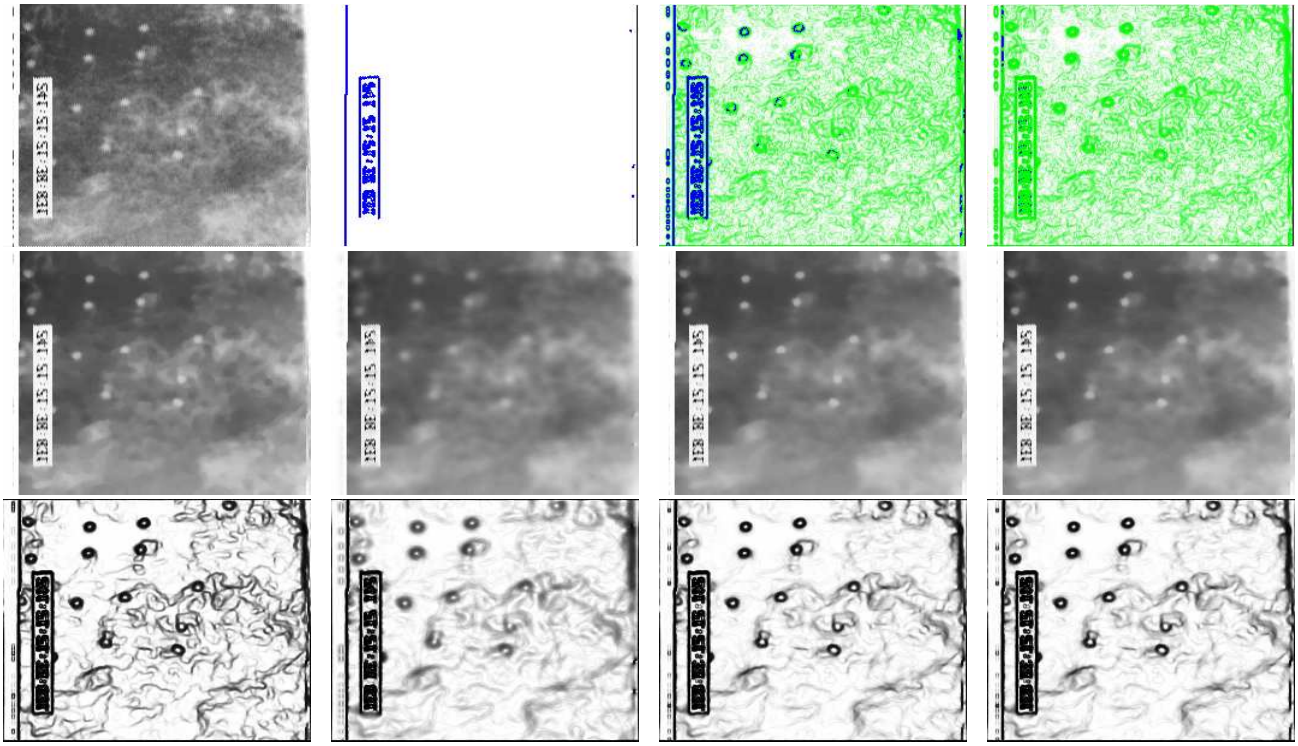

Figure 4: **First Column**: radar image of land mines, reconstructed image using TV-based diffusion only and corresponding edge map, iterations=500; **Second Column**: direction map, reconstruction, and edge map using (1), threshold $\epsilon = 25$, iterations $= 100$; **Third Column**: direction map, reconstruction, and edge map using the proposed model (4-5), threshold $\epsilon = 25$, iterations=500; **Fourth Column**: direction map, reconstruction, and edge map using the proposed model (4-5), threshold $\epsilon = 100$, iterations $= 500$; (all images: $c, k = 0.025$, spatial resolution $= 256\times256$)

highly successful in recovering both piecewise smooth and degraded images.

Appendix: Existence of a solution to (4-5)

Properties of ϕ:

Recall that the set of functions of bounded variation is defined as

$$BV(\Omega) := \{u \in L^1(\Omega) \mid \int_\Omega |Du| < \infty\}.$$

where

$$\int_\Omega |Du| := \sup_{\phi \in A}\{\int_\Omega f(x)\mathrm{div}\phi(x)dx\}$$

and

$$A := \{\phi \in C_0^1(\Omega, R^n)|\ |\phi(x)| \leq 1,\ on\ \Omega\}.$$

$Du = \nabla u \cdot \mathcal{L}^n + D^s u$ is a Radon measure, where ∇u is the density of the absolutely continuous part of Du with respect to the n-dimensional Lebesgue measure, $\mathcal{L}^n$, and $D^s u$ is the singular part (see [14]). Therefore, we can define

$$\int_\Omega \phi(x, Dv) := \int_\Omega \phi(x, \nabla u)dx + \int_\Omega |D^s v|$$

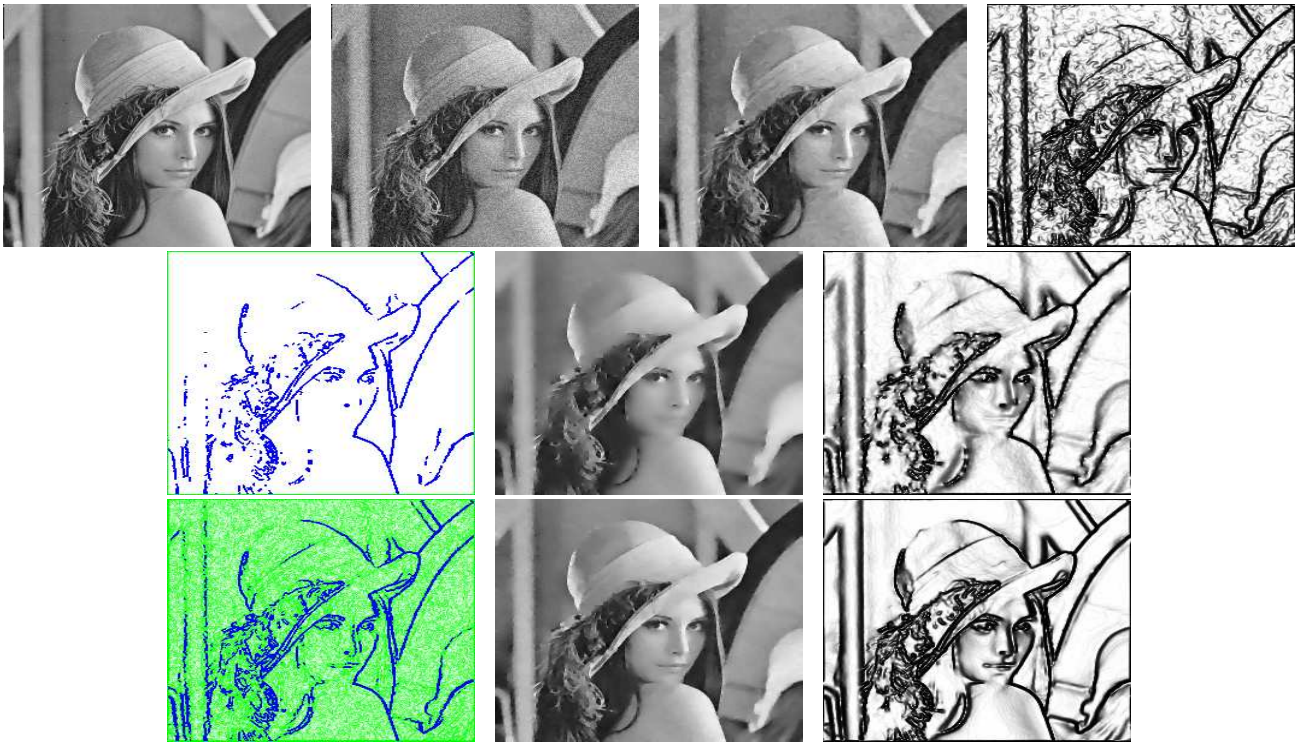

Figure 5: **First Row**: true image, image + noise, reconstruction and edge map using TV restoration; **Second Row**: direction map, reconstruction, and edge map using (1); **Third Row**: direction map, reconstruction, and edge map using the proposed model (4-5); (all images: threshold $\epsilon = 17$, iterations=500, $c, k = 0.025$, spatial resolution = 256×256)

where ϕ is defined as in (5). Straightforward calculations give the following lemma:

Lemma 5.1 *For all $u \in BV(\Omega)$,*

$$\int_\Omega \phi(x, Du) = \sup_\psi \int_\Omega \left(-u \mathrm{div}\psi - \frac{p(x)-1}{p(x)} |\psi|^{\frac{p(x)}{p(x)-1}} \right) dx \tag{11}$$

where ϕ is defined using (5) and the supremum is taken over all $\psi \in C^1(\Omega, \mathbf{R}^n)$ with $|\psi| \leq 1$.

Lemma 5.2 *(lower semi-continuity) If $v_j, v \in BV(\Omega)$ satisfy $v_j \to v$ in $L^1(\Omega)$ as $j \to \infty$ then*

$$\Phi_\lambda(v) \leq \Phi_\lambda(v_j). \tag{12}$$

where

$$\Phi_\lambda(v) := \int_\Omega \phi(x, Dv) + \frac{\lambda}{2} \int_\Omega |v - I|^2 dx \tag{13}$$

for $I \in BV(\Omega) \cap L^2(\Omega)$ and ϕ defined as in (5).

Lower semi-continuity (lemma 5.2) is a direct consequence of lemma 5.1.

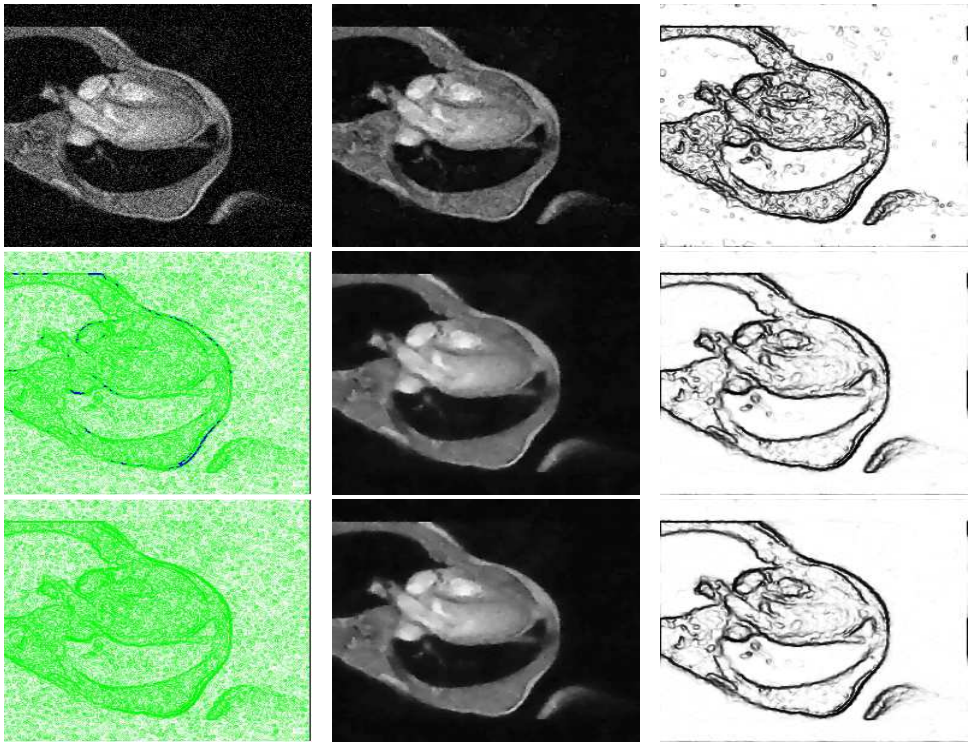

Figure 6: **First Row**, MRI image of a heart with Gaussian noise (SNR=1:3), reconstruction and edge map using TV only, iterations = 2000; **Second Row**, direction map, reconstruction, and edge map using (4)-(5) with threshold $\epsilon = 50$, iterations = 850; **Third Row**, direction map, reconstruction, and edge map using (4)-(5) with threshold $\epsilon = 150$, iterations = 850; (all images: $c, k = 0.0075$, spatial resolution = 256×256)

The Minimization Problem

Theorem 5.3 *Suppose $I \in BV(\Omega) \cap L^2(\Omega)$ where Ω is an open bounded subset of $\mathbf{R}^n$ with Lipshitz boundary. Then there exists a unique solution to the minimization problem*

$$\min\{\Phi_\lambda(v) \,:\, v \in BV(\Omega) \cap L^2(\Omega)\}. \tag{14}$$

Proof: Let $\{u_n\}$ be a minimizing sequence of (14) in $BV(\Omega) \cap L^2(\Omega)$. Since $\{u_n\}$ is bounded in $BV(\Omega)$ and $L^2(\Omega)$, using the compactness of $BV(\Omega)$ and the weak compactness of $L^2(\Omega)$, there exists a subsequence $\{u_{n_k}\}$ of $\{u_n\}$ and a function $u \in BV(\Omega) \cap L^2(\Omega)$ satisfying

$$u_{n_k} \to u \text{ strongly in } L^1(\Omega) \tag{15}$$

$$u_{n_k} \rightharpoonup u \text{ weakly in } L^2(\Omega). \tag{16}$$

By lemma 5.2, we have that

$$\Phi_\lambda(u) \le \liminf_{k\to\infty} \Phi_\lambda(u_{n_k}) = \inf_{BV(\Omega)\cap L^2(\Omega)} \Phi_\lambda(v).$$

Hence, u is a solution of the minimization problem. Uniqueness follows from the strict convexity of Φ_λ.

Existence, Uniqueness and Long Time Behavior

Theorem 5.4 *Suppose $u_0 \in L^\infty(\Omega) \cap BV(\Omega)$ and ϕ is defined as in (5). Then there exists a unique weak solution $u \in L^\infty(0, T; BV(\Omega) \cap L^\infty(\Omega))$ of (6)-(8) with $\dot{u} \in L^2(\Omega \times [0, T])$ and $u(0) = u_0$.*

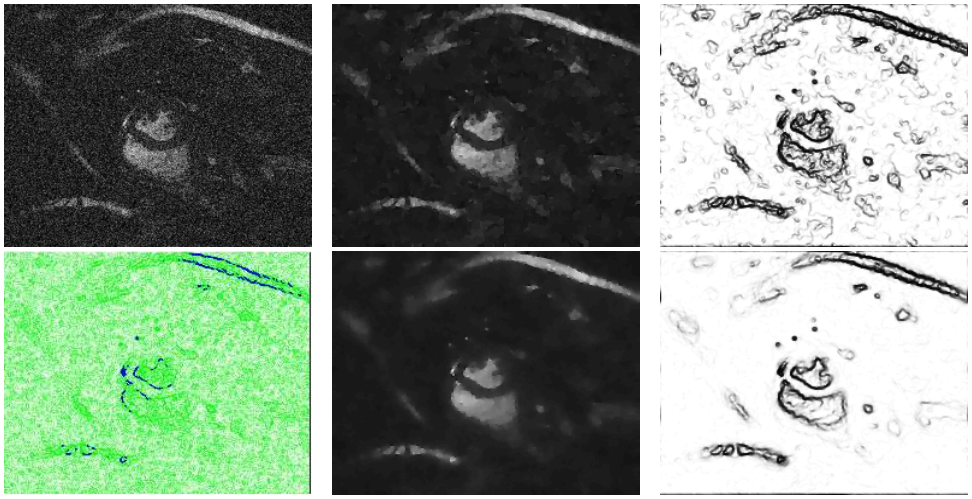

Figure 7: **First Row**: MRI image with noise acquired through the instrument, reconstruction and edge map using TV restoration, iterations = 2000; **Second Row Row**: direction map, reconstruction, and edge map using the proposed model (4-5), threshold $\epsilon = 30$, iterations = 1000 (all images: $c, k = 0.0075$, spatial resolution = 208×256)

Theorem 5.5 *As $t \to \infty$, the weak solution of (6)-(8) weakly converges in $BV(\Omega) \cap L^2(\Omega)$ to a minimizer $\overline{u}$ of Φ_λ.*

See [11] for the proofs of lemma 5.1 and theorems 5.4 and 5.5.

Acknowledgments

The authors would like to thank Sebastien Barre for the MRI heart image in figure 6, Mark Griswald for the MRI image in figure 7, and Michael Ramsey for the ASTER image in figure 8.

References

[1] R. Acar and C. R. Vogel. Analysis of bounded variation penalty methods for ill-posed problems. *Inverse Problems*, 10(6):1217–1229, 1994.

[2] L. Alvarez, P.-L. Lions, and J.-M. Morel. Image selective smoothing and edge detection by nonlinear diffusion. II. *SIAM J. Numer. Anal.*, 29(3):845–866, 1992.

[3] G. Aubert and L. Vese. A variational method in image recovery. *SIAM J. Numer. Anal.*, 34(5):1948–1979, 1997.

[4] P. Blomgren. Total variation methods for restoration of vector valued images. *Ph.D. Thesis*, pages 384–387, 1998.

[5] P. Blomgren, T. F. Chan, P. Mulet, L. Vese, and W. L. Wan. Variational PDE models and methods for image processing. In *Numerical analysis 1999 (Dundee)*, volume 420 of *Chapman & Hall/CRC Res. Notes Math.*, pages 43–67. Chapman & Hall/CRC, Boca Raton, FL, 2000.

[6] P. Blomgren, T. F. Chan, P. Mulet, and C. Wong. Total variation image restoration: Numerical methods and extensions. *Proceedings of the 1997 IEEE International Conference on Image Processing*, III:384–387, 1997.

[7] A. Brook, R. Kimmel, and N. A. Sochen. Variational restoration and edge detection for color images. *J. Math. Imaging Vision*, 18(3):247–268, 2003.

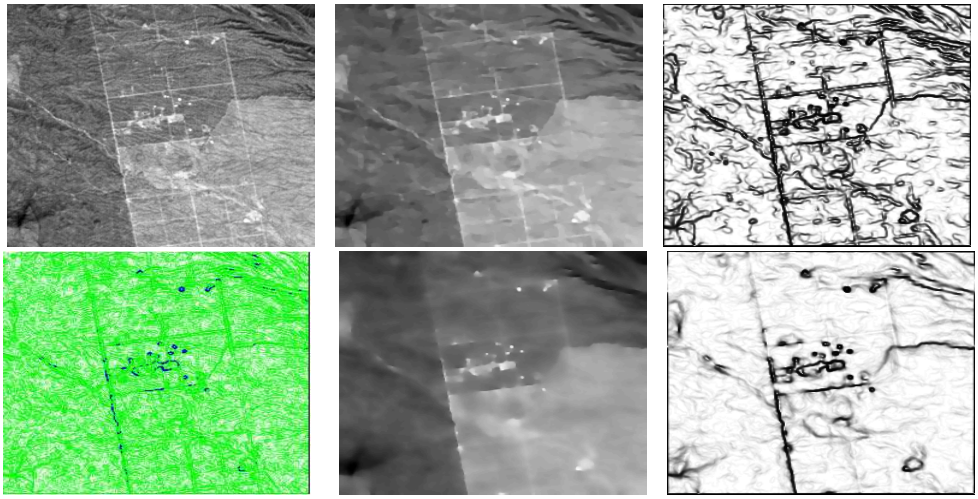

Figure 8: **First Row**: true image, reconstruction and edge map using TV restoration, iterations = 1000; **Second Row Row**: direction map, reconstruction, and edge map using the proposed model (4-5) with threshold $\epsilon = 30$, iterations = 500; (all reconstructions: $c, k = 0.025$, spatial resolution = 256×256)

[8] F. Catté, P.-L. Lions, J.-M. Morel, and T. Coll. Image selective smoothing and edge detection by nonlinear diffusion. *SIAM J. Numer. Anal.*, 29(1):182–193, 1992.

[9] A. Chambolle and P.-L. Lions. Image recovery via total variation minimization and related problems. *Numer. Math.*, 76(2):167–188, 1997.

[10] Y. Chen and S. Levine. Image recovery via diffusion tensor and time-delay regularization. *Journal of Visual Communications and Image Representation*, 13:156–175, 2002.

[11] Y. Chen, S. E. Levine, and M. Rao. Functionals with $p(x)$-growth in image restoration. *Preprint*, 2004.

[12] G.-H. Cottet and M. E. Ayyadi. A volterra type model for image processing. *IEEE Trans. Image Process.*, 7(3):292–303, 1998.

[13] G.-H. Cottet and L. Germain. Image processing through reaction combined with nonlinear diffusion. *Math. Comp.*, 61(204):659–673, 1993.

[14] L. C. Evans and R. F. Gariepy. *Measure theory and fine properties of functions*. Studies in Advanced Mathematics. CRC Press, Boca Raton, FL, 1992.

[15] R. Malladi and J. Sethian. Image-processing: Flows under min/max curvature and mean-curvature. *GMIP*, 58(2):127–141, March 1996.

[16] R. Malladi, J. Sethian, and B. Vemuri. Shape modeling with front propagation: A level set approach. *PAMI*, 17(2):158–175, February 1995.

[17] D. Mumford and J. Shah. Optimal approximations by piecewise smooth functions and associated variational problems. *Comm. Pure Appl. Math.*, 42(5):577–685, 1989.

[18] M. Nitzberg and T. Shiota. Nonlinear image filtering with edge and corner enhancement. *PAMI*, 14(8):826–833, August 1992.

[19] S. Osher and J. A. Sethian. Fronts propagating with curvature-dependent speed: algorithms based on Hamilton-Jacobi formulations. *J. Comput. Phys.*, 79(1):12–49, 1988.

[20] P. Perona and J. Malik. Scale-space and edge detection using anisotropic diffusion. *IEEE Transactions on Pattern Analysis and Machine Intelligence*, 12:629–639, 1990.

[21] L. Rudin and S. Osher. Total variation based image restoration with free local constraints. *Proc. IEEE ICIP, Vol. I, Austin, Texas*, pages 629–639, 1994.

[22] L. Rudin, S. Osher, and E. Fatemi. Nonlinear total variation based noise removal algorithms. *Physica D*, 60:259–268, 1992.

[23] C. Schnörr. A study of a convex variational diffusion approach for image segmentation and feature extraction. *J. Math. Imaging Vision*, 8(3):271–292, 1998.

[24] J. A. Sethian. *Level set methods*, volume 3 of *Cambridge Monographs on Applied and Computational Mathematics*. Cambridge University Press, Cambridge, 1996. Evolving interfaces in geometry, fluid mechanics, computer vision, and materials science.

[25] N. Sochen, R. Kimmel, and R. Malladi. A general framework for low level vision. *IEEE Trans. Image Process.*, 7(3):310–3112–412–4998, 1998.

[26] D. M. Strong and T. F. Chan. Spatially and scale adaptive total variation based regularization and anisotropic diffusion in image processing. *Technical Report, Univeristy of California, Los Angeles, CA*, CAM96-46, 1996.

[27] C. R. Vogel and M. E. Oman. Iterative methods for total variation denoising. *SIAM J. Sci. Comput.*, 17(1):227–238, 1996. Special issue on iterative methods in numerical linear algebra (Breckenridge, CO, 1994).

[28] J. Weickert. Scale-space properties of nonlinear diffusion filtering with a diffusion tensor. *Report No. 110. Laboratory of Technomathematics, University of Kaiserslautern, Germany*, 1994.

[29] J. Weickert. Mulitscale texture enhancement. In *Compuer Analysis of Images and Patterns*, pages 230–237. Lecture Notes in Computer Science, Vol. 970 Springer, Berlin, 1995.